Large-area single-crystal sheets of borophene on Cu(111) surfaces

Rongting Wu[1,2], Ilya K. Drozdov[3], Stephen Eltinge[4], Percy Zahl[3], Sohrab Ismail-Beigi[1,4,5], Ivan Božović[1,2,3] and Adrian Gozar[1,2] *

[1] Department of Applied Physics, Yale University, New Haven, CT 06520, USA
[2] Energy Sciences Institute, Yale University, West Haven, CT 06516, USA
[3] Brookhaven National Laboratory, Upton, NY 11973, USA
[4] Department of Physics, Yale University, New Haven, CT 06520, USA
[5] Department of Mechanical Engineering & Materials Science, Yale University, New Haven, CT 06520, USA

Borophene, a theoretically proposed two-dimensional boron allotrope[1-3], has attracted much attention[4,5] as a candidate material platform for high-speed, transparent, and flexible electronics[6-9]. It has been recently synthesized, on Ag(111) substrates[10,11], and studied by tunneling and electron spectroscopy[12]. However, the exact crystal structure is still controversial, the nanometer size single-crystal domains produced so far are too small for device fabrication, and the structural tunability *via* substrate-dependent epitaxy is yet to be proven. We report on synthesis of borophene monitored *in situ* by low-energy electron microscopy, diffraction and scanning tunneling microscopy and modeled by *ab initio* theory. We resolve the crystal structure and phase diagram of borophene on Ag(111) but find that the domains remain nanoscale for all growth conditions. However, by growing borophene on Cu(111) surfaces, we obtain large single-crystal domains, up to 100 μm^2 in size. The crystal structure is a novel triangular network with $\eta = 1/5$ concentration of hexagonal vacancies. Our experimental data together with first principles calculations indicate charge-transfer coupling to substrate without significant covalent bonding. Our work sets the stage for fabricating borophene-based devices and substantiates the idea of borophene as a model for artificial 2D materials development.

Metallic sheets of atomically thin borophene are expected to enable new functionalities of two-dimensional (2D) materials and open applications in flexible electronics and near-visible plasmonics[5,13]. The polymorphism of borophene also opens up concrete paths for engineering structural and electronic properties of anisotropic 2D metallic sheets[1,5-7] by choosing different substrates or growth conditions. Atomic boron planes isostructural to graphene already stand out by providing a high critical superconducting temperature ($T_c \approx$ 40 K) in MgB_2, making the prospect of discovering other boron-based 2D superconducting compounds promising[14].

Using Ag(111) substrates and molecular beam epitaxy, a pioneering work demonstrated successful synthesis of atomically thin 2D boron layers organized in islands tens of nanometers in size[10,11]. Indications for persisting Dirac fermions are present in photoemission

data[12,15] of this boron sheet and their existence is supported by theoretical calculations in several polymorphs[14]. To the extent that simple tight binding approximations provide a good parametrization for *ab initio* band structure calculations in borophene, it is notable that within nearest-neighbor interaction the degeneracy at graphene K points and the presence of associated Dirac cones are preserved for an arbitrary distribution of 'impurity' atoms filling the hexagonal centers of any type of super-cell of a honeycomb lattice. This remains true in higher order hopping for several of the theoretically stable sheets of borophene with the concomitant appearance of flat or weakly dispersive bands arising from localized orbitals of the center atoms. This peculiarity of the honeycomb lattice is interesting because flat bands can engender strange, non-Fermi-Liquid metals, and perhaps open a path to room-temperature superconductivity[16]. In order to realize this potential, it is pressing to explore synthesis of borophene on other substrates and study the ensuing crystal structures.

Notwithstanding the promises for unique electronic and mechanical properties, the lateral extent of borophene domains produced so far makes them amenable to study by only few techniques and is far below the limits required for device fabrication. This is an impediment for gaining access to key properties, such as resistivity, Hall effect, magnetoresistance, etc., because micron-sized single-crystal flakes are needed for such measurements. Here, we solve this challenge by growing borophene on a different substrate (copper), producing single-crystal domains 10-100 μm^2 in size. Elemental borophene may now be used as a material platform to make devices and study fundamental physics.

The interest in borophene encounters substantial theoretical and experimental challenges. The prediction and targeted synthesis of borophene is a delicate affair because of the existence of many states with energies very close to the overall minimum[1-3,7,8]. Furthermore, it has been predicted that the already rich phase space for 2D borophene sheets in vacuum can be easily modified by the interaction with the substrate of choice[13]. 2D phases are found to be stabilized by the existence of boron vacancies in a triangular lattice but theory predicts a disconnect between the stable patterns of vacancies in free-standing and metal-supported borophene[13]. This is important for the transfer of sheets from metallic to device-compatible substrates.

In this work we utilize the capabilities of Low Energy Electron Microscopy (LEEM) for simultaneous real-time monitoring of dynamics of borophene nucleation and growth as well as k-space structural characterization by Low Energy Electron Diffraction (LEED)[17-20]. A setup employing a customized electron-beam evaporation source along with other sample preparation capabilities (see Methods) enables precise control of deposition rates, which is essential for producing crystalline 2D sheets. In order to determine the structure of borophene on Cu(111) we performed high-resolution scanning tunneling microscopy (STM) measurements[21] using functionalized tips[22,23] in conjunction with *ab initio* density functional theory (DFT) calculations[24-26].

We first studied the growth and stability of borophene on Ag(111) surfaces in detail. Previous work used STM data in combination with DFT to infer the crystal structure[10,11]. For a given 2D borophene sheet, the parameter η is defined[1] as the ratio of vacant hexagon-

center sites to the number of triangular lattice sites in a unit cell (UC). An 'empty' honeycomb (graphene-like) lattice has $\eta = 1/3$, and a putative all-boron triangular lattice has $\eta = 0$. For borophene on Ag(111), two structures denoted β_{12} and χ_3 have been proposed, corresponding to $\eta = 1/6$ and $\eta = 1/5$, respectively. We have synthesized borophene layers on Ag(111) at various substrate temperatures (Fig. 1). Both β_{12} and χ_3 phases were indeed identified by LEED, and we confirm that the former is favored at lower growth temperatures, 550 K $\lesssim$ T $\lesssim$ 600 K. Nevertheless, weak diffraction peaks corresponding to the χ_3 phase are also present, indicating phase coexistence in this temperature range. Growth at an elevated temperature, 650 K $\lesssim$ T $\lesssim$ 720 K, renders only the χ_3 phase (Fig. 1c). Further increasing the substrate temperature generates additional orientations for χ_3 domains, rotated by 30°, as well as a re-entrance of the β_{12} phase, also with domains rotated by 30° (see Fig.1d and Supplementary Figs. S1 and S2). In-situ post-growth temperature ramps in the 550–850 K and 750–910 K ranges (Fig. 1e,f) both show that the χ_3 phase is more stable than the β_{12} counterpart.

Figs. 1b and 1c show bright-field LEEM and LEED images of borophene on Ag(111). The size of single-crystal domains is only in the range of tens of nm. The domains do not coalesce and the average size does not change even at complete monolayer (ML) coverage. These results are further confirmed by atomic force microscopy (AFM) (Fig. S3). The higher nucleating density on Ag surfaces along with a tendency for boron clustering could be a limiting factor for the average domain size. Indeed, continuing deposition beyond one full ML coverage leads to a reduction of crystallinity (dark areas in Fig. 1d). The bright areas in the same panel correspond to regions where nano-sized β_{12}-30°, χ_3-30° and χ_3 domains are found to coexist and, occasionally, even overlap with each other spatially (dark-field images in Supplementary Fig. S4).

In order to produce larger domains, we have explored candidate substrates less inert than Ag, i.e., potentially able to promote growth of larger domains, but not so reactive as to form metal boride compounds. Our data support the notion that Cu substrates achieve this balance. Fig. 2 illustrates nucleation and growth of a large area ML film of borophene on a single-crystal Cu(111) substrate, at T = 770 K and at the rate of 0.05 ML/min (see the supplementary movie "B-Cu(111) Film Growth"). The growth on lower terraces of Cu step edges is anisotropic and proceeds at a rate that is about five times faster along the step edge than in the perpendicular direction (Supplementary Fig. S5). Nucleation on upper terraces follows subsequently and displays more isotropic growth kinetics. Growth of single crystals ensues once the density of nucleation sites reaches a saturation value observed to be around $0.75/\mu m^2$. Ambient AFM data (Fig. 2b-d) corroborate the growth of one-atom-thick borophene islands.

LEED and dark-field LEEM images in Fig. 3 show that the borophene sheets are composed of large single-crystal domains. The domain length along the terrace directions can exceed 10 μm. Domain widths in the perpendicular direction can be limited by the terrace width, typically 1-3 μm and determined by the angle of surface miscut with respect to the Cu(111) plane. Nevertheless, boundaries of borophene domains do not always follow the Cu terraces, and it is common to find borophene flakes that cross many steps edges (Supplementary Fig. S6). In spite of the large number of Bragg peaks in the LEED data, we observe

that many of them 'light up' the same domain structure. We elucidate this domain structure by performing μLEED. Fig. 3 and Fig. S6 demonstrate that the entire ML is made out of six domain types. They are obtained by 120° rotations of two types of UCs with different chiralities (Fig. 3i), and correspond to a single structural phase. The UC of our structure is 21.84 Å × 15.96 Å in size, larger than those corresponding to β_{12} and χ_3 sheets, and is rotated by a small angle (± 5.8°) with respect to the [100] direction of the Cu(111) surface (Fig. 3h). While domain sizes are generally correlated with substrate step edges, large individual Cu terraces also allow faceted islands growth (Supplementary Fig. S7 and Supplementary Movie "B-Cu111 Faceted Islands"). Important and delicate questions involving possible boride formation, B-Cu solubility or the role of evaporation and sub-surface dissolution are also elegantly solved using LEEM capabilities: we are able to induce subsurface dissolution and resurfacing of crystalline borophene sheets by thermal cycling the Cu(111) substrate covered by a full ML of borophene (see Supplementary Fig. S8 and Supplementary Movie "B-Cu(111) Miscibility").

To decipher the internal structure of the UC, we performed STM measurements and *ab initio* density functional theory (DFT) calculations. Fig. 3j and Figs. 4a,b show large area topographic STM images of a borophene domain on Cu terraces. The Fourier transform of the topographic signal is in very good agreement with LEED results indicating that the same borophene structure is preserved at T = 5 K. STM tip functionalization with carbon monoxide molecules[21,22] dramatically improves the spatial resolution compared to what is typically achieved with bare metallic tips (Supplementary Fig. S10). Such ultra-resolved STM data allow us to propose an array of potential planar borophene sheets whose stabilities are subsequently found by DFT calculations and relaxations[24,25]. Fig. 4e-g summarizes this procedure and display our proposed structure of borophene on Cu(111) substrates, which is also the one with the largest binding energy of all the sheets investigated. The good agreement between the experimental (Fig. 4e) and DFT simulated structure using tunneling states with p_z character[26] for the functionalized STM tip (Fig. 4f) supports this assignment (see Supplementary Information Sections 3 and 4). The proposed structure has a boron vacancy density of $\eta = 1/5$ (the same as the χ_3 structure).

Our *ab initio* calculations reveal a rather flat sheet of relaxed borophene with a z-corrugation of only 0.43 Å, consistent with prior theoretically investigated structures on Cu(111) with smaller UCs[13,27]. The average boron-boron bond length is 1.72 Å, with a spread < 0.2 Å, which indicates that the sheet on Cu(111) is under anisotropic, ≈4% on the average, tensile strain compared to the corresponding structure relaxed in vacuum. More details on other borophene structures we investigated can be found in Section 4 of the Supplementary Information. We investigated the film-substrate interaction, a relevant parameter for prospective sheet transfer and device fabrication (Fig. 5). The calculations show that our borophene structure in Fig. 4 is electron doped via charge transfer with no significant covalent bonding. The value of $\eta = 1/5$ can be understood if one takes into account that the self-doping mechanism[3,28] in conjunction with the electron transfer from Cu to B is expected to increase η above $\eta \approx 1/9$ (maximum stability for isolated sheets). Our experimental findings are generally in agreement with the predicted behavior of 2D boron on Cu(111) surfaces[13,27] and confirm the predictive power and capabilities of *ab initio* calculations for

guiding future choices of material substrates for structural and electronic engineering of 2D sheets of borophene.

Data on both Cu and Ag substrates indicate that the formation of atomically thin 2D boron sheets is a self-limiting process; this is advantageous for synthesis of heterostructures based on atomically thin layers. Indeed, beyond 1 ML coverage, the growth rate on Cu and Ag decreases dramatically, even if the boron flux is substantially increased. Next, our study illustrates several other differences brought about by the material choice for the substrate. Growth dynamics, the influence of incoming atomic flux or substrate temperature on the structure, film adhesion and rippling[10,11,29,30] are shown to be very different on the two substrates. This is crucial from the device fabrication perspective, because synthesis of large-size domains is required for engineering heterostructures. Our results underscore the importance of borophene-substrate interactions and the choice of substrate materials. Simultaneous real- and k-space mapping is shown to be very useful for controlled synthesis and characterization of new 2D phases, and in conjunction with several elemental sources can also be used to visualize heterostructure growth.

References

1. Tang, H. & Ismail-Beigi, S. Novel precursors for boron nanotubes: the competition of two-center and three center bonding in boron sheets. *Phys. Rev. Lett.* **99**, 115501 (2007).
2. Yang, X., Ding, Y. & Ni, J., Ab initio prediction of stable boron sheets and boron nanotubes: structure, stability and electronic properties. *Phys. Rev. B* **77**, 041402(R) (2008).
3. Tang, H. & Ismail-Beigi, S. Self-doping in boron sheets from first principles: a route to structural design of metal boride nanostructures. *Phys. Rev. B* **80**, 134113 (2009)
4. Mannix, A. J., Kiraly, B., Hersam, M. C. & Guisinger, N. P. Synthesis and chemistry of elemental 2D materials. *Nature Chemistry* **1**, 0014 (2017).
5. Mannix, A. J., Zhang, Z., Guisinger, N. P., Yakobson, B. I., & Hersam, M. C. Borophene as a prototype for synthetic 2D materials development. *Nature Nanotechnology* **13**, 444-450 (2018).
6. Zhang, Z. H., Penev, E. S. & Yakobson, B. I. Polyphony in B flat. *Nature Chemistry* **8**, 525-527 (2016).
7. Penev, E. S., Bhowmick, S., Sadrzadeh, A. & Yakobson, B. I. Polymorphism of Two-Dimensional Boron. *Nano Letters* **12**, 2441-2445 (2012).
8. Wu, X., Dai, J., Zhao, Y., Zhuo, Z., Yang, J. & Zeng X. C. Two-Dimensional Boron Monolayer Sheets. *ACS Nano* **6** 7443-7453 (2012).
9. Zhang, Z., Yang, Y., Penev, E. S. & Yakobson, B. I. Elasticity, flexibility and ideal strength of borophenes, *Adv. Func. Mat.* 1605059 (2017).
10. Mannix, A. J., *et al.* Synthesis of borophenes: Anisotropic, two-dimensional boron polymorphs. *Science* **350**, 1513-1516 (2015).
11. Feng, B., et al. Experimental realization of two-dimensional boron sheets. *Nature Chemistry* 8, 563 (2016).
12. Feng, B. J., *et al.* Direct evidence of metallic bands in a monolayer boron sheet. *Physical Review B* **94**, 041408 (2016).
13. Zhang, Z. H., Yang, Y., Gao, G. Y. & Yakobson, B. I. Two-Dimensional Boron Monolayers Mediated by Metal Substrates. *Angew. Chem. Int. Ed.* **54**, 13022-13026 (2015).
14. Penev, E. S., Kutana, A. & Yakobson, B. I. Can Two-Dimensional Boron Superconduct? *Nano Letters* **16**, 2522-2526 (2016).
15. Feng, B., Sugino, O., *et al.*, Dirac fermions in borophene. *Phys. Rev. Lett.* **118**, 096401 (2017).
16. Volovik, G. E. From standard model of particle physics to room-temperature superconductivity, *Phys. Scr*. **T164**, 014014 (2015).
17. Bauer, E., Low energy electron microscopy. Rep. Progr. Phys. 57, 895-938 (1994).

18. Hannon, J. B. & Tromp, R. M. Low-energy microscopy of surface phase transitions. *Annu. Rev. Mater. Res*. **33**, 263 (2003).
19. Suter, P., Sadowski, J. T. & Sutter, E. Graphene on Pt(111): growth and substrate interaction. *Phys. Rev. B* **80**, 245411 (2009).
20. Altman, M. S., Trends in low energy electron microscopy. *J. Phys. Condens. Matter* **22**, 084017 (2010).
21. Giessibl, F. J. High-speed force sensor for force microscopy and profilometry utilizing a quartz tuning fork. *Appl. Phys. Lett*. **73**, 3956-3958 (1998).
22. Gross, L., Moll, N., Mohn, F., Curioni, A., Meyer, G., Hanke, F. & Persson, M. High-resolution molecular orbital imaging using a p-wave STM tip. *Phys. Rev. Lett*. **107**, 086101 (2011).
23. Hapala, P., Kichin, Wagner, C., G., Tautz, Temirov, R., F. S. & Jelinek P. Mechanism of high resolution STM/AFM imaging with functionalized tips. Phys. Rev. B **90**, 085421 (2014).
24. Gianozzi, P. et al., Quantum Espresso: a modular and open source software project for quantum simulations of materials. *J. Phys.: Condens. Matter* **21**, 395502 (2009).
25. Tersoff, J. & Hamann, D. R Theory and Application for the scanning tunneling microscope. Phys. Rev. Lett. 50, 1998 (1983).
26. Chen, C. J. Tunneling matrix elements in three dimensional space: the derivative rule and the sum rule. *Phys. Rev. B* 42, 8841 (1990).
27. Liu, H. S., Gao, J. F. & Zhao, J. J. From Boron Cluster to Two-Dimensional Boron Sheet on Cu(111) Surface: Growth Mechanism and Hole Formation. *Scientific Reports* **3**, 3238 (2013).
28. Galeev, T. R., Chen, Q. et al., Deciphering the mystery of hexagon holes in an all boron graphene α-sheet. *Phys. Chem. Chem. Phys.* **13**, 11575-11578 (2011).
29. Zhang, Z., Mannix, A. J., Hu, Z., Kiraly, B., Guisinger, N. P., Hersam, M. C. & Yakobson, B. I. Substrate induced nanoscale undulations of borophene on Silver. *Nano Letters* 16, 6622-6627 (2016).
30. Liu, X., Zhang, Z., Wang, L., Yakobson, B.I. & Hersam, M.C. Intermixing and periodic self-assembly of borophene line defects. *Nature Materials* **17**, 2018 https://doi.org/10.1038/s41563-018-0134-1

Acknowledgements

This research was supported by the U.S. Department of Energy, Basic Energy Sciences, Materials Sciences and Engineering Division. R.W. and A.G. are supported by the Gordon and Betty Moore Foundation's EPiQS Initiative through Grant GBMF4410. I.K.D. acknowledges the support of the BNL Gertrude and Maurice Goldhaber Distinguished Fellowship. This research used resources of the Center for Functional Nanomaterials, which is a U.S. DOE Office of Science Facility, at Brookhaven National Laboratory under Contract No. DE-SC0012704. S.E. is supported by the National Science Foundation Graduate Research Fellowship through Grant DGE-1122492. S.E and S.I-B thank computing resources provided by the staff of the Yale University Faculty of Arts and Sciences High Performance Computing Center as well as NSF XSEDE resources via Grant TG-MCA08X007.

Author contributions

R.T. took and analyzed the experimental LEEM/LEED/XPS/AFM data with help from A.G.. I.K.D. and P.Z. acquired the low temperature STM data and analyzed them with help from R.T. and A.G.. S.E. and S.I-B. performed the ab initio calculations and analyzed the results. I.B. conceived and supervised the project. A.G. wrote the manuscript with contribution from all authors.

Additional information

Supplementary information is available in the online version of the paper. Reprints and permission information is available online at www.nature.com/reprints. Correspondence and requests for materials should be addressed to A.G.

Competing financial interests
The authors declare no competing financial interests.

Correspondence (*)
adrian.gozar@yale.edu

Figure captions

Figure 1 | Structure of borophene grown on Ag(111) surfaces. **a**, The top, real-space image, shows the terraced surface of the pristine Ag substrate revealed by LEEM phase contrast. The corresponding LEED pattern is shown at the bottom. **b**, LEEM image of surface morphology (top) for 1 ML coverage and the corresponding LEED pattern (bottom) showing that borophene growth at T = 570 K yields primarily the β_{12} structure (blue rectangles) with a weak contribution from χ_3 domains (green triangle). **c**, LEEM and LEED images as in panel b for borophene growth at T = 720 K which yields only the χ_3 structure. The diffraction pattern (green triangle in the bottom panel) shows that the χ_3 UC corresponds to a 3×3 reconstruction of the Ag(111) surface. **d**, LEEM and LEED images for borophene growth at T = 750 K which generates both β_{12} and χ_3 structures. Two additional UC orientations rotated by 30° with respect to LEED images in panels b and c appear at this temperature. The rotated structures, denoted by β_{12}-R30 and χ_3-R30, are shown as yellow rectangles and purple triangles, respectively. **e**. Temperature-dependent intensity of the diffraction peaks across the white shaded line profile at the bottom of panel b. The data show the evolution of borophene structures during heating from T = 570 K to 840 K. **f**, Temperature-dependent diffraction peak intensities along the white lines in the bottom of panel d. The data show the evolution with heating from T = 760 K to 910 K.

Figure 2 | Growth dynamics of borophene on Cu(111) surface. a, Sequence of bright-field LEEM images at T = 770 K reveal that borophene islands prefer to nucleate from the down-step edge of Cu terraces (i.e. the direction marked by the arrow in the first, t = 0s, panel) and that growth proceeds faster along the step-edge direction: ~97 Å/s compared to ~ 20 Å/s for the perpendicular direction (see also Supplementary Fig. S5). Snapshots taken at 75s and 228s illustrate that at this stage of growth borophene flakes display sharp edges along low-index directions of the substrate, as shown by the white arrows (see also Supplementary Movie "B-Cu111 Triangular Islands"). These two panels along with the snapshot at 468s also show that down-step nucleation is followed by borophene growth across the upper step edge. In contrast to the down-step growth, up-step growth generates arc-shaped islands, indicating more isotropic growth kinetics, see the white arrow in the 468s panel. A continuous monolayer (ML) emerges reproducing faithfully the Cu(111) terrace structure. The growth rate was ~ 0.05 ML/min (see also Supplementary Movie "B-Cu111 Film Growth"). **b**, Topographic Atomic Force Microscopy (AFM) image around 0.1 ML coverage. The surface RMS is 0.24 Å on Cu(111) terraces and 0.43 Å on borophene islands (green arrows), respectively. **c**, Line profile (corresponding to the black line in panel b showing a 2.8 Å tall atomic step of the Cu substrate. **d**, Line profile corresponding to the blue line in panel b showing that the thickness of the borophene sheet in ambient conditions is around 3.0 Å. **e**, Ex-situ X-ray Photoemission (XPS) spectra from a B/Cu(111) sample. The data indicate that after one hour exposure to air about 80% of borophene has been oxidized, see also Supplementary Fig. S9.

Figure 3 | Domain structure of borophene on Cu(111) revealed by selected area diffraction. **a**, Bright-field LEEM image for borophene on Cu(111) at about 0.4 ML surface coverage. Borophene appears in yellow color. **b-d**, Selected area LEED patterns taken from single-crystal domains of borophene using an electron beam focused to 1.5 μm. The three different LEED patterns orientations correspond to three domain orientations which

can be connected by the 120° rotations. The large white rhombus corresponds to the Cu(111) substrate unit cell (UC) while smaller yellow rhomboid defines the borophene UC. **e-g**, Selected-area LEED patterns for the three remaining domains which are mirror-symmetric with respect to those depicted in panels b-d. The reciprocal UC of borophene is shown in green. The six domains in panels b-g share the same structure and exhaust the observed domain orientation variety for borophene on Cu(111). **h**, The two mirror symmetric UCs of borophene correspond to a ($\sqrt{73}\times\sqrt{39}$) R±5.8° superstructure on Cu(111). Yellow and green rhomboids are the real-space correspondents of the reciprocal UCs shown in b–d and e-g, respectively. **i**, combined dark-field images of a multi-domain flake of borophene. The color coding from panels b-g is carried through in panel i. **j**. A large area Scanning Tunneling Microscope (STM) image at about 0.5 ML borophene coverage. The boundary of a single domain (dark blue) is marked by a green dashed line. Other areas in this panel correspond to terraces of uncovered Cu(111). The inset shows a Fourier Transform of the STM signal from the area marked by white rectangle inside the borophene domain. The reciprocal space information obtained in this way is in agreement with electron diffraction data.

Figure 4 | The structure of borophene on Cu(111) as revealed by STM data and DFT simulations. **a**, Large area STM topographic image of a borophene-Cu step edge (setpoint parameters: I_s = 10 pA and V_b = +100mV). Color coding: borophene appears in yellow (higher z values) and is identified by the UC motif, displayed as a small blue rhomboid; Cu appears in dark blue (lower z values). The top drawing illustrates this layering sequence. **b**, Same as panel a but for a different z-stacking: here the scanning captures a borophene domain which most likely nucleated from a down step edge of a Cu terrace, see discussion in Fig. 2. **c**, **d**, show profiles across the blue and red lines in panels a and b, respectively. The height difference between borophene and the top Cu layer is 1.4 Å in panel a and -0.6 Å in panel b, indicating a reduced density of states (DOS) in borophene with respect to Cu. **e**, Ultra-high resolution STM data of borophene (setpoint parameters: I_s = 50 pA and V_b = +20mV). The rhomboid corresponds to the borophene UC and the red dashed lines are guides along the zig-zag pattern characteristic of all STM data, see Supplementary Fig. S10. **f**, DFT simulated constant tunneling current iso-surface of the proposed borophene structure assuming a p_z tunneling state for the tip (Ref. 26). **g**, Pictorial view of the borophene structure with B atoms and bonds shown in green. The red dashed lines continue the basic zig-zag motif from panel e through the DFT simulations (panel f) and the proposed balls-and-sticks structure (panel g).

Figure 5 | Charge-transfer interaction between borophene and Cu(111) surface. **a**, Electronic DOS for the relaxed borophene sheet on Cu (green solid curve), for the same structure relaxed in vacuum ('free' borophene – green dotted curve) and for Cu (pink curve). Shaded area corresponds to the occupied states for the undoped free borophene. DFT calculations show that relaxed B/Cu(111) is electron doped by 0.23 e/B atom. The vertical dashed marks the Fermi level (E_F) in B/Cu(111) as well as that of the isolated borophene if it were electron doped by 0.23 e/atom (this doping amount shifts E_F of the isolated borophene by 1.18 eV). The high similarity between the green curves indicates that the interaction between borophene and Cu is of a charge-transfer type with a minor degree of covalence. **b**, Iso-surface plot of charge redistribution between Cu planes (pink atoms) and relaxed borophene (green atoms) along the (100) direction of the underlying honeycomb lattice. Electron depletion is shown in purple and accumulation in yellow: electrons move from Cu d_{z2} into B p_z - like orbitals; this real-space image further confirms the

charge-transfer scenario and the lack of significant covalent bonding between borophene and Cu.

Methods

A. Low Energy Electron Microscopy of borophene growth on Cu(111) and Ag(111) surfaces. Growth of borophene on single crystal Cu(111) and Ag(111) substrates were performed in an ultrahigh-vacuum LEEM system (Elmitec LEEM-III) augmented with molecular beam epitaxy (MBE) capability. The base pressure is 2×10^{-10} Torr. Real-time monitoring of in-situ growth and of the atomic deposition rate were essential for achieving synthesis of high-quality single crystals and precise control of coverage. Single-crystal Cu(111) and Ag(111) (roughness < 10 nm, orientation accuracy < 0.1º, Princeton Scientific Co.) were cleaned by repeated cycles of argon ion sputtering and post-annealing at 870 K and 770 K respectively, until a clean and broad terraced structure, with corresponding bright and sharp LEED pattern, was observed. Boron was evaporated by an electron-beam evaporator with a power around 30W, focused onto a pure boron rod (purity 99.9999% from ESPI) with a diameter of 3 mm. Clean single-crystal Cu(111) and Ag(111) surfaces were kept at elevated temperature, while the LEEM images or LEED patterns were taken during or after the borophene growth process. Post-annealing of the different borophene structures on Ag(111) was performed in the same system, while the LEED patterns were recorded concurrently. For borophene grown at 570 K, post annealing from 570 K to 840 K was carried out with the temperature ramp-rate around 2.7 K/min while for borophene grown at 760 K, post annealing from 760 K to 910 K was carried out with the temperature ramp-rate around 3.4 K/min. In both cases the LEED images were recorded with a 5s per frame integration time.

B. X-ray Photoemission (XPS) and Atomic Force Microscopy (AFM) measurements. The XPS spectra were taken ex-situ using the monochromatic 1486.7 eV Al Kα X-ray source with a resolution of 0.47 eV. The energy was calibrated using the Cu $2p^{3/2}$ (932.67 eV) and Au $4f^{7/2}$ (84.00 eV) peaks on a clean copper plate and a gold foil. The instrument used is PHI VersaProbe II Scanning XPS Microprobe. The XPS peak fitting was done with CasaXPS software using a mixture of Gaussian (30%) and Lorentzian (70%) functions. AFM measurements were carried out in the tapping mode at ambient conditions using a Cypher S AFM from Asylum Research, and silicon tips with 10 nm apex radii.

C. Scanning Tunneling Microscopy (STM) data. These measurements were acquired with a customized Createc scanning tunneling and non-contact atomic force microscope (NC-AFM/STM) system operating in ultra-high vacuum and at a nominal temperature of T = 5K. The Pt/Ir tip was mounted on a qPlus sensor, Ref. 21, operating at 32 kHz was used for detection of NC-AFM signals. Pt/Ir tips were prepared by in-situ field emission on clean Au or Cu single crystal surfaces. In-situ Boron deposition on sputtered/annealed Cu(111) surfaces at T ~ 600º C was done in a preparation chamber equipped with a LN_2 cooled manipulator and a LEED system. Enhanced spatial resolution was achieved by metal tip functionalization, which was realized by in-situ dosing of carbon-monoxide

(CO) molecules and subsequent vertical manipulation. The measurements were performed using an open-source GXSM SPM control system (P. Zahl, T. Wagner "GXSM - Smart & Customizable SPM Control" Imaging & Microscopy (GIT), Jan. 26, 2015. http://gxsm.sourceforge.net/).

D. *Ab initio* calculations. *Ab initio* density functional theory calculations were performed using the Quantum ESPRESSO package (Ref. 24), using pseudopotentials generated with the Perdew–Zunger local density approximation to the exchange-correlation functional. A plane-wave basis set with an energy cutoff of 476 eV was used. For relaxations, the Brillouin zone was sampled at the Γ point, and for DOS calculations a 9×9×1 Monkhorst–Pack grid was used. Boron atoms were relaxed until forces were less than 2.5×10^{-3} eV/Å. For calculations on a copper surface, the borophene sheet was relaxed on a two-layer slab of copper at its experimental bulk lattice parameter. STM calculations were performed using the Tersoff–Hamann formalism, with *p*-type orbitals described using the derivative rule of Chen (Refs. 25, 26).

Data availability

All data generated and analyzed during this study are included in this published article and associated Supplementary Information.

FIGURE 1

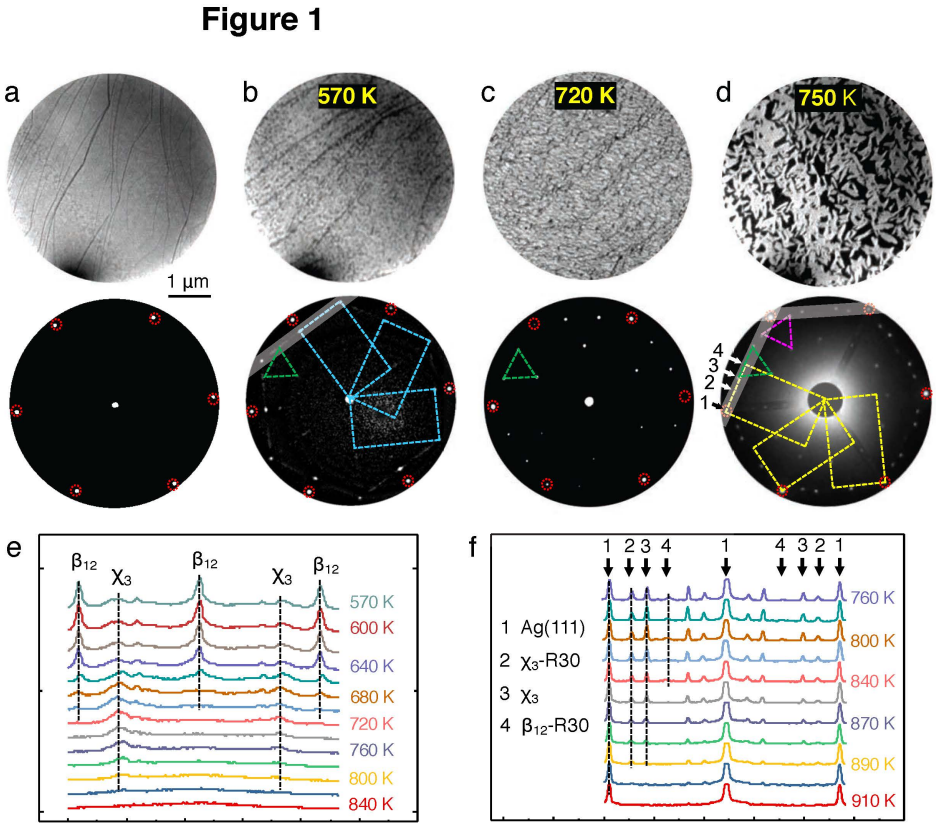
Figure 1
a
b
570 K
c
720 K
d
750 K
1 μm
4
3
2
1
e
β12
X3
β12
X3
β12
570 K
600 K
640 K
680 K
720 K
760 K
800 K
840 K
f
1 2 3 4
1
4 3 2 1
1 Ag(111)
2 X3-R30
3 X3
4 β12-R30
760 K
800 K
840 K
870 K
890 K
910 K

FIGURE 2

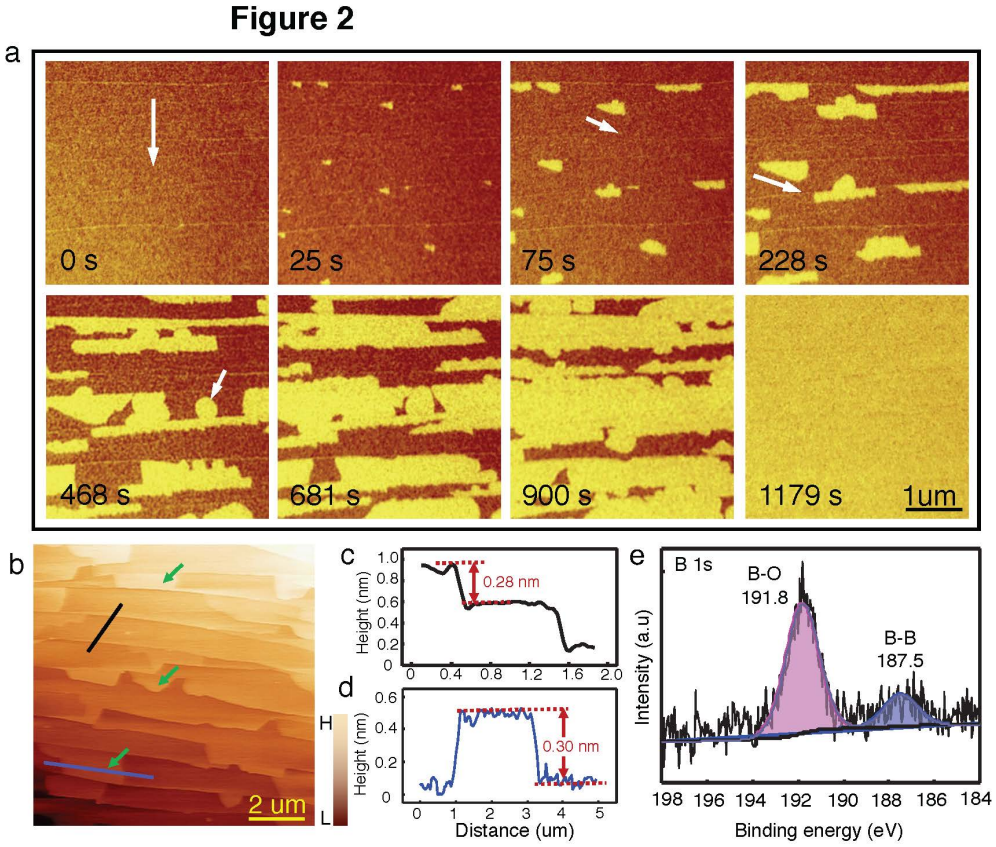
Figure 2
a
0 s
25 s
75 s
228 s
468 s
681 s
900 s
1179 s
1um
b
2 um
H
L
c
Height (nm)
0.28 nm
Distance (um)
d
Height (nm)
0.30 nm
e
B 1s
B-O
191.8
B-B
187.5
Intensity (a.u)
Binding energy (eV)

FIGURE 3

Figure 3

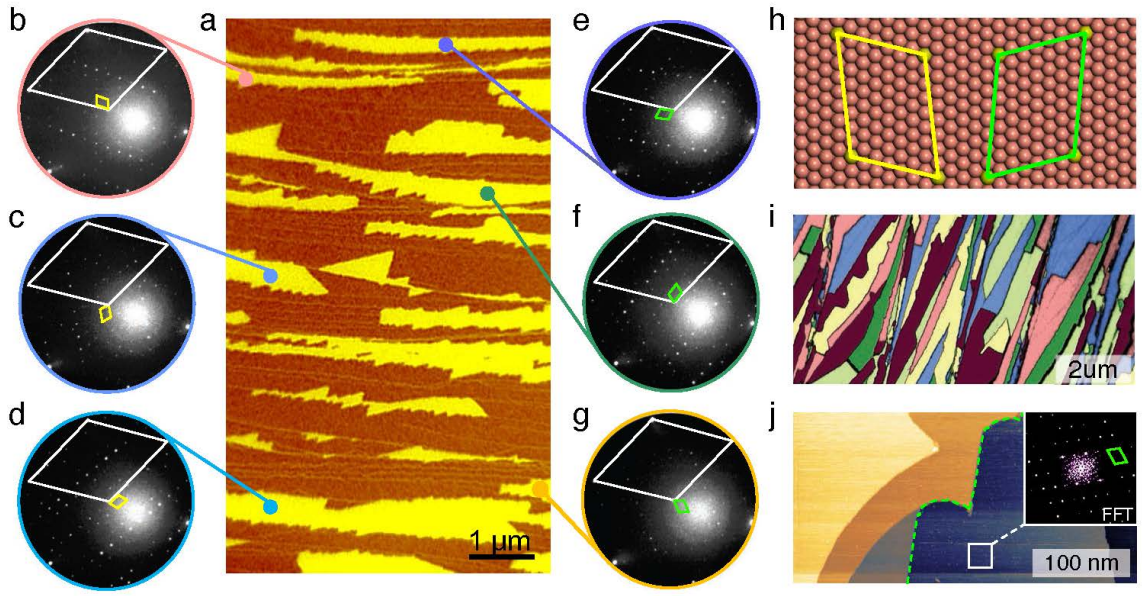

FIGURE 4

Figure 4

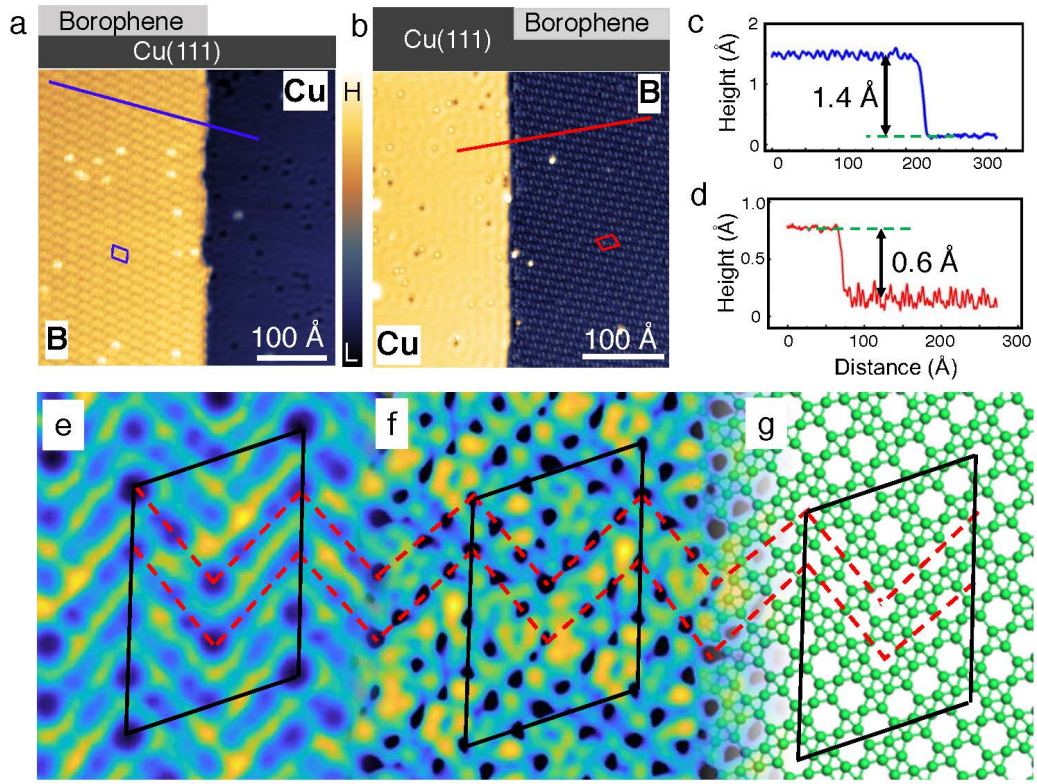

FIGURE 5

Figure 5